Chapter 6

Dielectric and Mechanical properties of Nb doped $CaCu_3Ti_4O_{12}$ / Poly(vinylidene fluoride) composites

The present chapter describes the structural, dielectric and mechanical properties of Nb doped CCTO/ PVDF composites. Nb doped $CaCu_3Ti_4O_{12}$ (NbCCTO) has been synthesised by solid state technique. 10, 20 and 50 wt% of Nb doped CCTO powder dispersed PVDF (PVDF-NbC) composites have been prepared by melt extrusion method. It is found that NbCCTO dispersion in PVDF improves the thermal, dielectric as well as mechanical properties of PVDF-NbC composites.

6. Results and discussion

6.1. Structural Analysis

X-ray diffraction patterns of NbCCTO, PVDF and their composites containing 10, 20 and 50 wt % NbCCTO in PVDF matrix have been shown in Fig 6.1. In case of NbCCTO, the diffraction peaks corresponding to reflections (220), (310), (222), (321), (400), (422) and (440) at 2θ values of 34.2°, 38.5°, 42.3°, 45.8°, 49.2°, 61.3° and 72.2° respectively confirm the formation of single phase compound [Sinclair et al (2002)]. No secondary phase is present. Pure PVDF crystallizes in α phase with characteristic 2θ peaks at 17.7°, 18.7°and 19.9° corresponding to (110), (020) and (111) crystal planes respectively [Varma et al (2010)]. Intensity of three major peaks (220), (400) and (422) of NbCCTO increases with increasing amount of NbCCTO in the composites. Predominance of NbCCTO phase can be seen in PVDF-50NbC composite indicated by suppressed diffraction peaks of PVDF. Average crystallite size determined for PVDF-50NbC composite from broadening of x-ray diffraction peak corresponding to (220) reflection using Scherrer's formula has been reduced to 47 nm from 59 nm for pure NbCCTO.

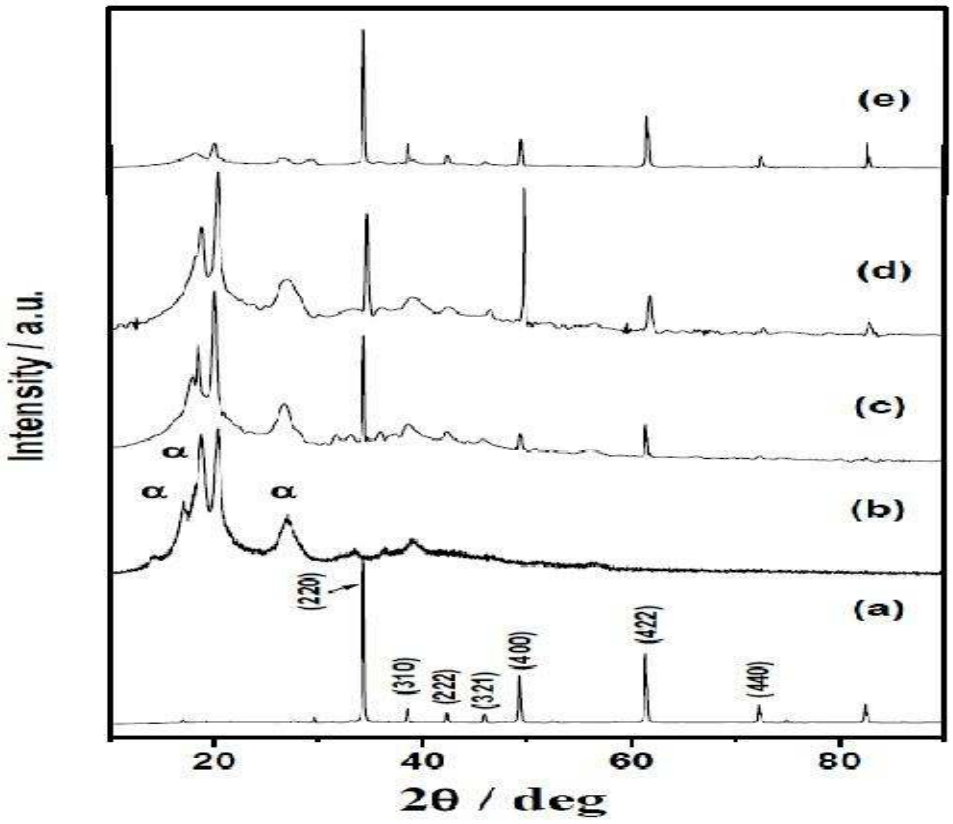

Figure 6.1 X-ray diffraction patterns for (a) NbCCTO, (b) PVDF, (c) PVDF-10NbC, (d) PVDF-20NbC and (e) PVDF-50NbC composites.

6.2 Surface morphology

SEM micrographs of pure PVDF and PVDF-NbC composites are shown in Fig 6.2. It is observed that the spherulitic morphology of pure PVDF is significantly altered by the presence of NbCCTO. Discrete particles of NbCCTO are observed for lower content of the ceramic in the composite (PVDF-10NbC). Aggregation of ceramic particles occurs for higher weight fraction of NbCCTO leading to connected network structure of NbCCTO in PVDF-50NbC composite.

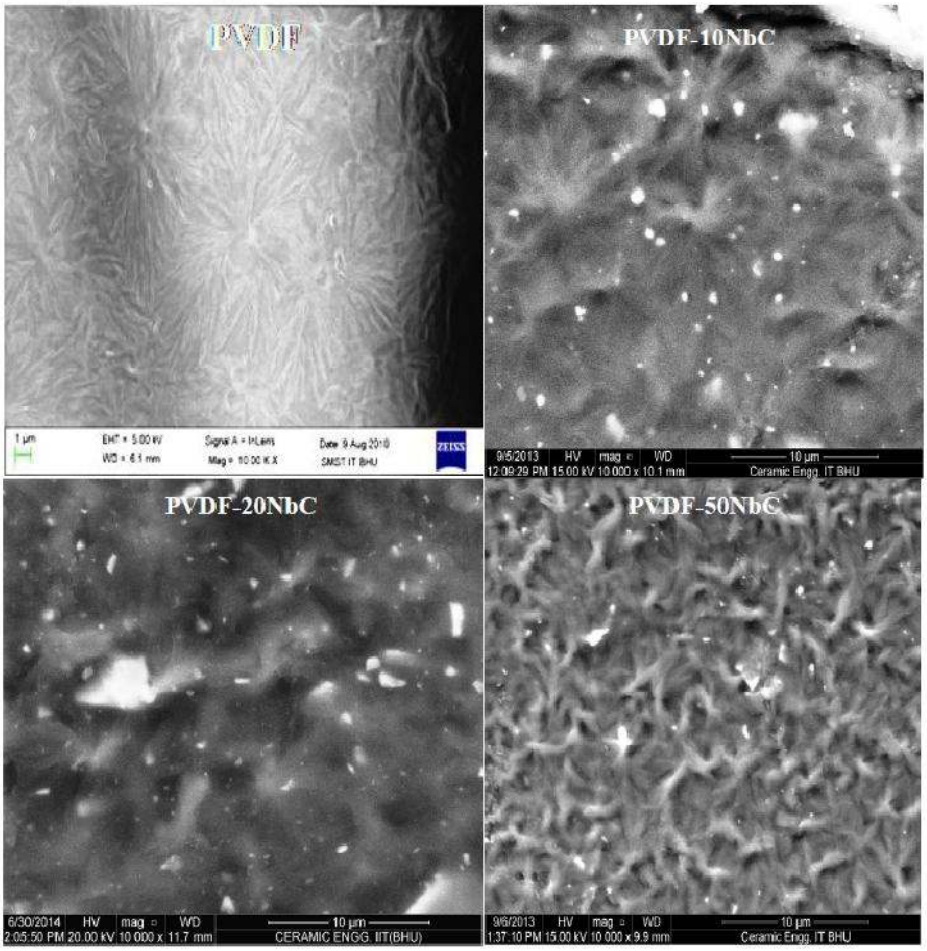

Figure 6.2 Scanning electron micrographs of PVDF, PVDF-10NbC, PVDF-20NbC and PVDF-50NbC composites.

6.3 Thermal behaviour

Thermogravimetric analysis (TGA) has been done to study the thermal stability of the polymer and the composites. Thermograms recorded for the pure PVDF and its composites are shown in Fig 5.3. It is observed that pure PVDF is stable up to 400°C and complete degradation of the polymer occurs at around 500°C. NbCCTO filler shifts the degradation temperature to higher side i.e. from 442^0C in PVDF to 442^0C, 460^0C and 480^0C in PVDF-10NbC, PVDF-20NbC and PVDF-50NbC respectively. It shows dispersion of NbCCTO improves the thermal stability of the composites.

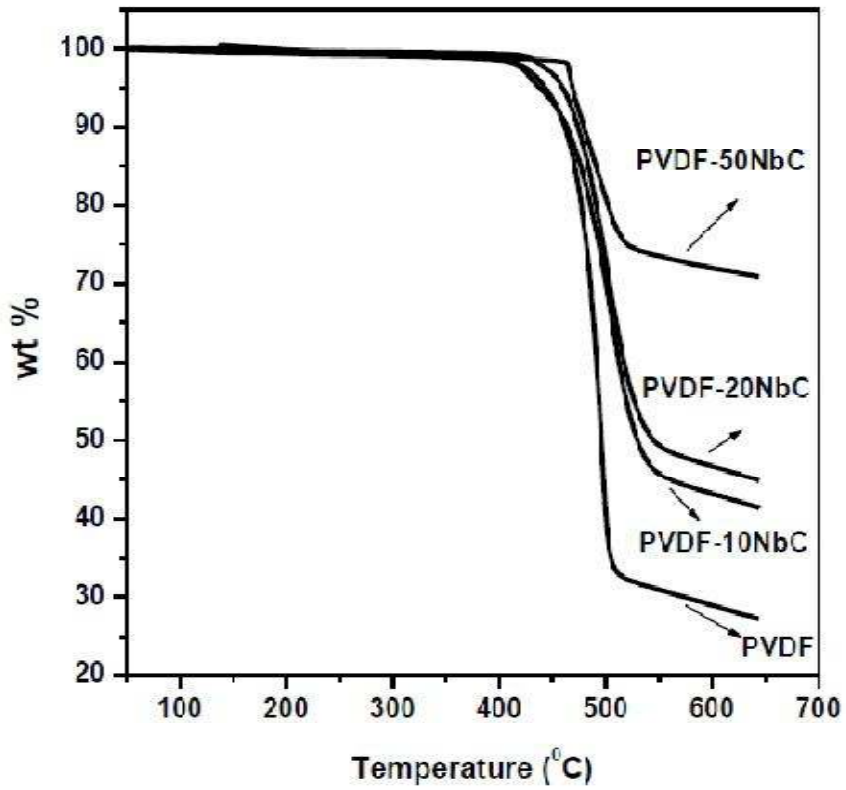

Figure 6.3 TGA of pure PVDF, PVDF-10NbC, PVDF-20NbC and PVDF-50NbC composites.

6.4. Mechanical properties

Figure 6.4 (a) shows the stress-strain curves of PVDF and its composites. Three samples are tested for each composition and average is taken. Young's modulus calculated from the slope of the linear region of the plots increases considerably. For PVDF, PVDF-10NbC, PVDF-20NbC and PVDF-50NbC, the values are 752, 760, 867, 1033 MPa, respectively showing continuous increase with increasing NbCCTO content (Fig 6.4 b). This increase in Young's modulus with increase in the weight percent of filler can be attributed to interaction between stiffer ceramic particles and PVDF matrix making composites stiffer as compared to pure PVDF. Elongation at breaking point decreases from 30% in PVDF to 20%, 18% and 16% in PVDF-10NbC, PVDF-20NbC and PVDF-50NbC composites respectively (Fig 6.4 c). This increase in the Young's

modulus with filler content can be attributed to increase in the resistance to the free movement of the polymeric chains by much harder ceramic particles. This is also a reason for decrease in elongation at the breaking point with increasing concentration of ceramic in the PVDF matrix.

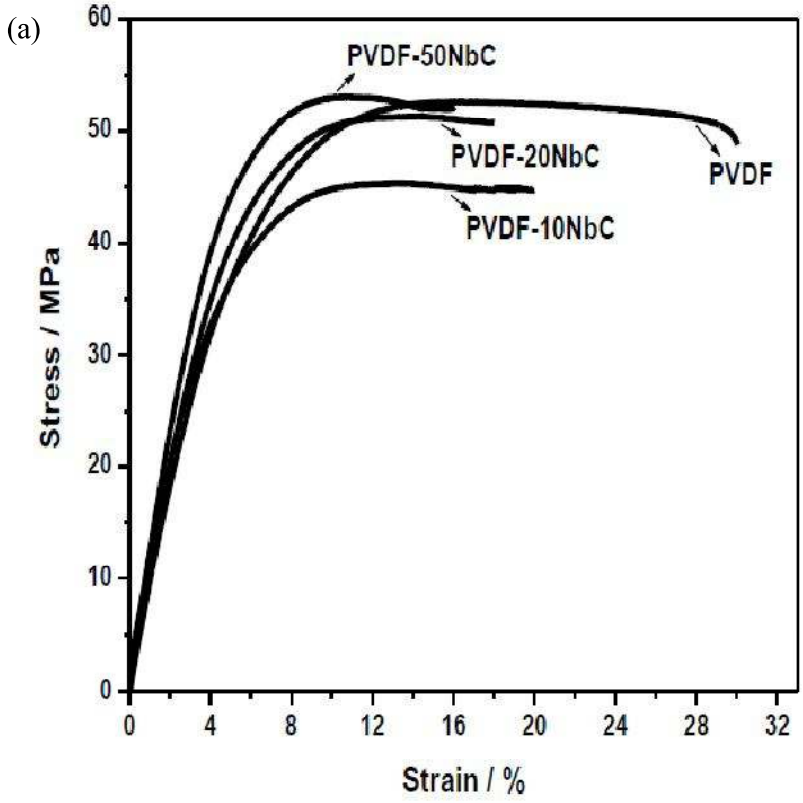

Figure 6.4 (a) Stress-strain curves for pure PVDF, PVDF-10NbC, PVDF-20NbC and PVDF-50NbC composites

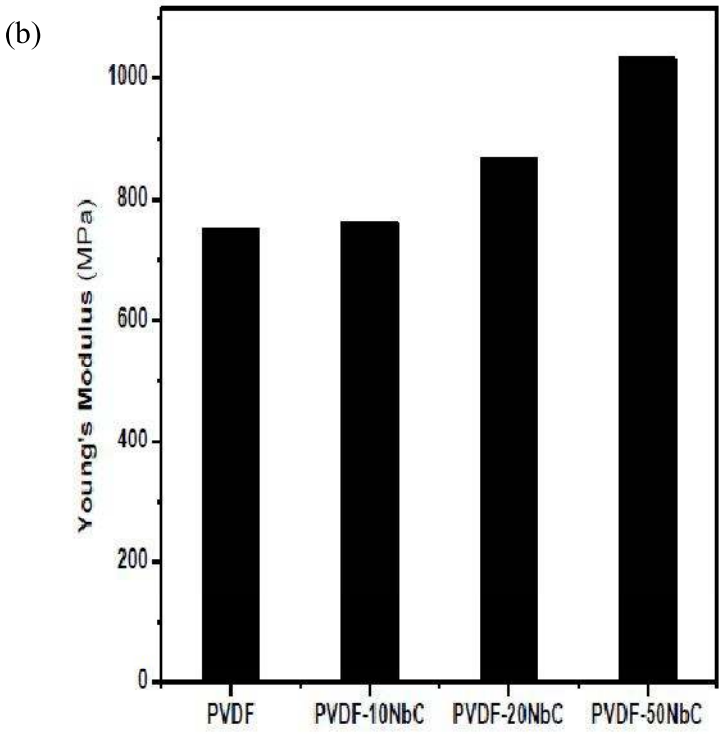

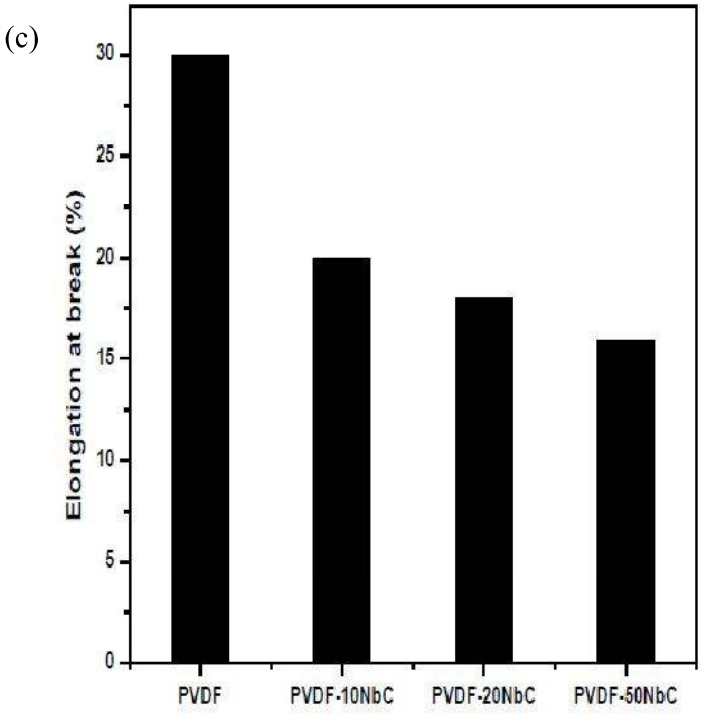

Figure 6.4 (b) Young's modulus of PVDF and composites and (c) Elongation at breaking point of PVDF and composites.

6.5. Dielectric properties

Frequency dependence of dielectric permittivity ε' of CCTO and NbCCTO is shown in fig 6.5 (a). ε' of CCTO was found to be 3100 at 100 Hz at room temperature. On doping with Nb, ε' increases to 25,500 at 100 Hz. CCTO as well as NbCCTO exhibits high ε' due to formation of barrier layers at the grains-grain boundaries interfaces [Sinclair et al (2002)]. In NbCCTO there is steep rise in the ε' at around 10^3-10^4 Hz, it seems that interfacial polarization effect is more dominant in NbCCTO than CCTO. ε' increases with temperature in PVDF, it is 3 at 40^0C and 100 Hz which increases to 8 at 120^0C and 100 Hz (Fig 6.5 c). In composites dielectric permittivity ε' increases with increasing content of NbCCTO in PVDF (Fig. 6.5 e). ε' at 40^0C and 100 Hz for PVDF, PVDF-10NbC PVDF-20NbC and PVDF-50NbC are 3.0, 20, 29 and 98 respectively. In all the cases, ε' obtained for composites is much higher than that of pure PVDF. PVDF is present in α phase only, which is non-polar. Due to the non-polar nature of PVDF, the value of ε' is low. ε' increases with decreasing frequency and vice versa. Increase in ε' with decreasing frequency is due to presence of interfacial polarization which plays an important role for its enhancement in the low frequency region. Composite materials always have microhetrogeneties due to presence of two or more phases in electrical contact. There exist a difference in the conductivity of the dispersed phase/phases and the matrix. This gives rise to interfacial or space charge polarization due to interaction of the charge carriers at the polymer-ceramic interface. Space charge polarization involves displacement of charge carriers over large distance. Hence it cannot follow the alternating field at high frequency. This gives rise to rapid decrease in ε' with increase in frequency in the low frequency region. Variation of ε' with frequency at a few temperature for all the compositions is shown in figs 6.5 (c, g, i and k). Figs 6.5 (g, i and k) shows similar behavior i.e. initially a rapid decrease in ε' with frequency in the low frequency region followed by a plateau above a certain frequency. It is important to note that ε' does not change much over the frequency range 10^2-10^6 Hz. It is desirable feature for use in device.

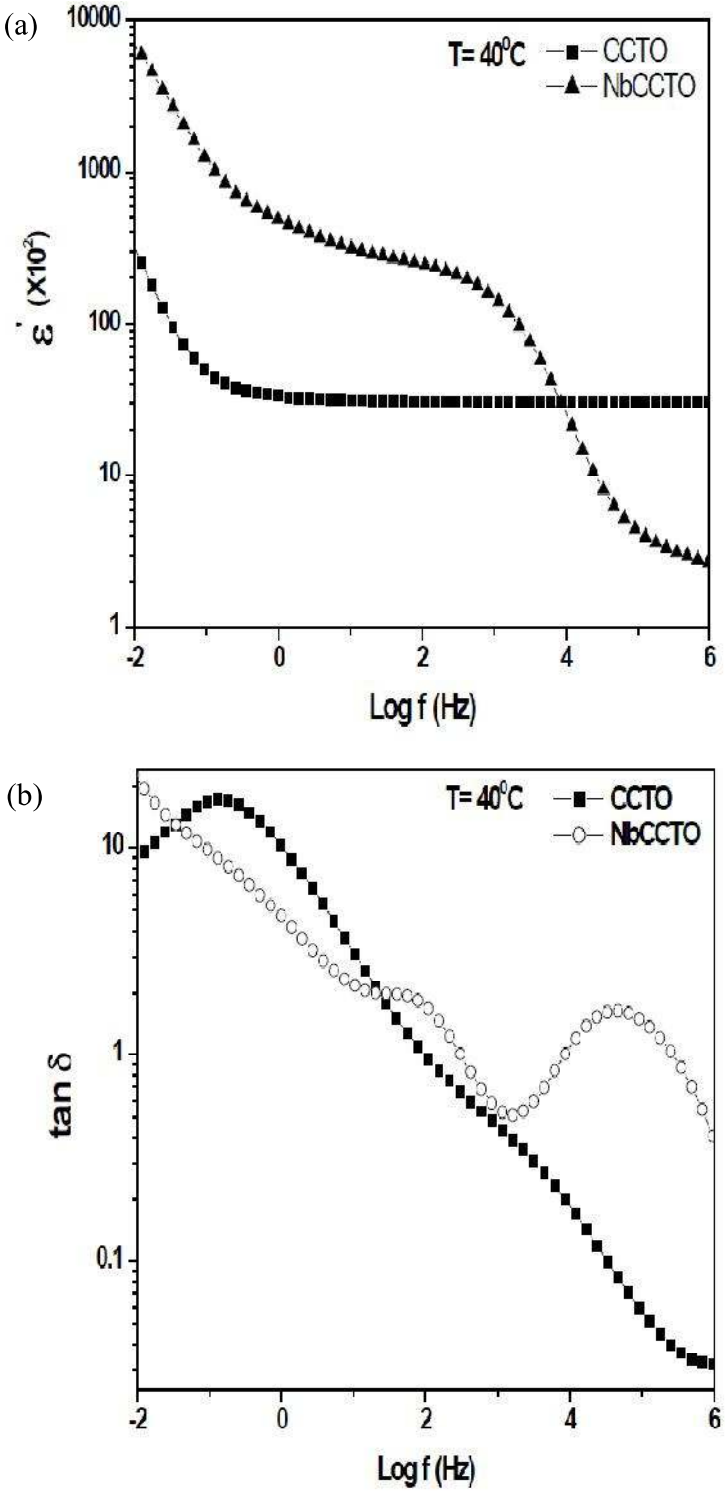

Figure 6.5 Frequency dependence of dielectric permittivity and tan δ (a and b) of CCTO and NbCCTO at 40^0C.

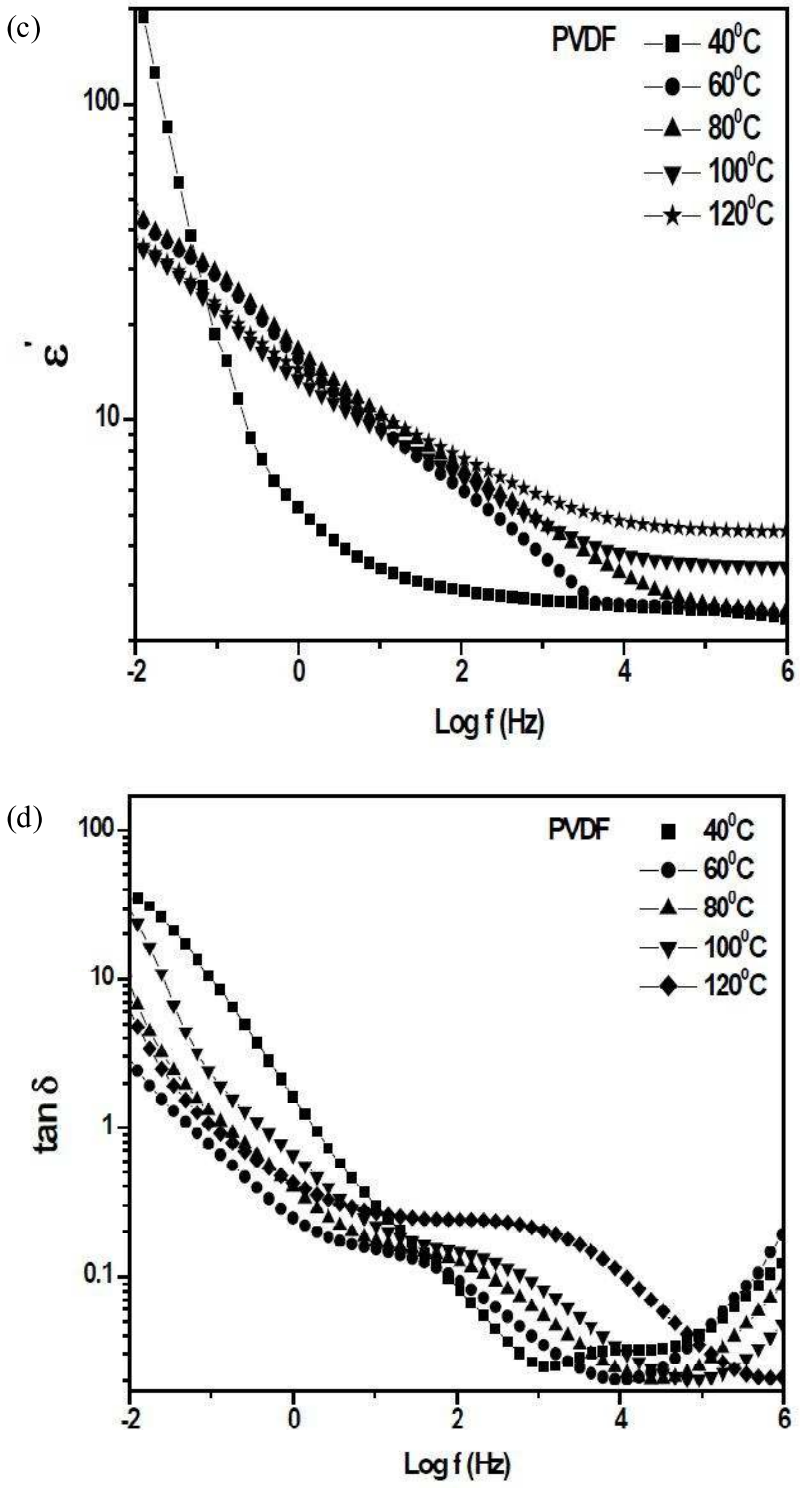

Figure 6.5 Frequency dependence of dielectric permittivity and tan δ (c and d) of PVDF at different temperatures.

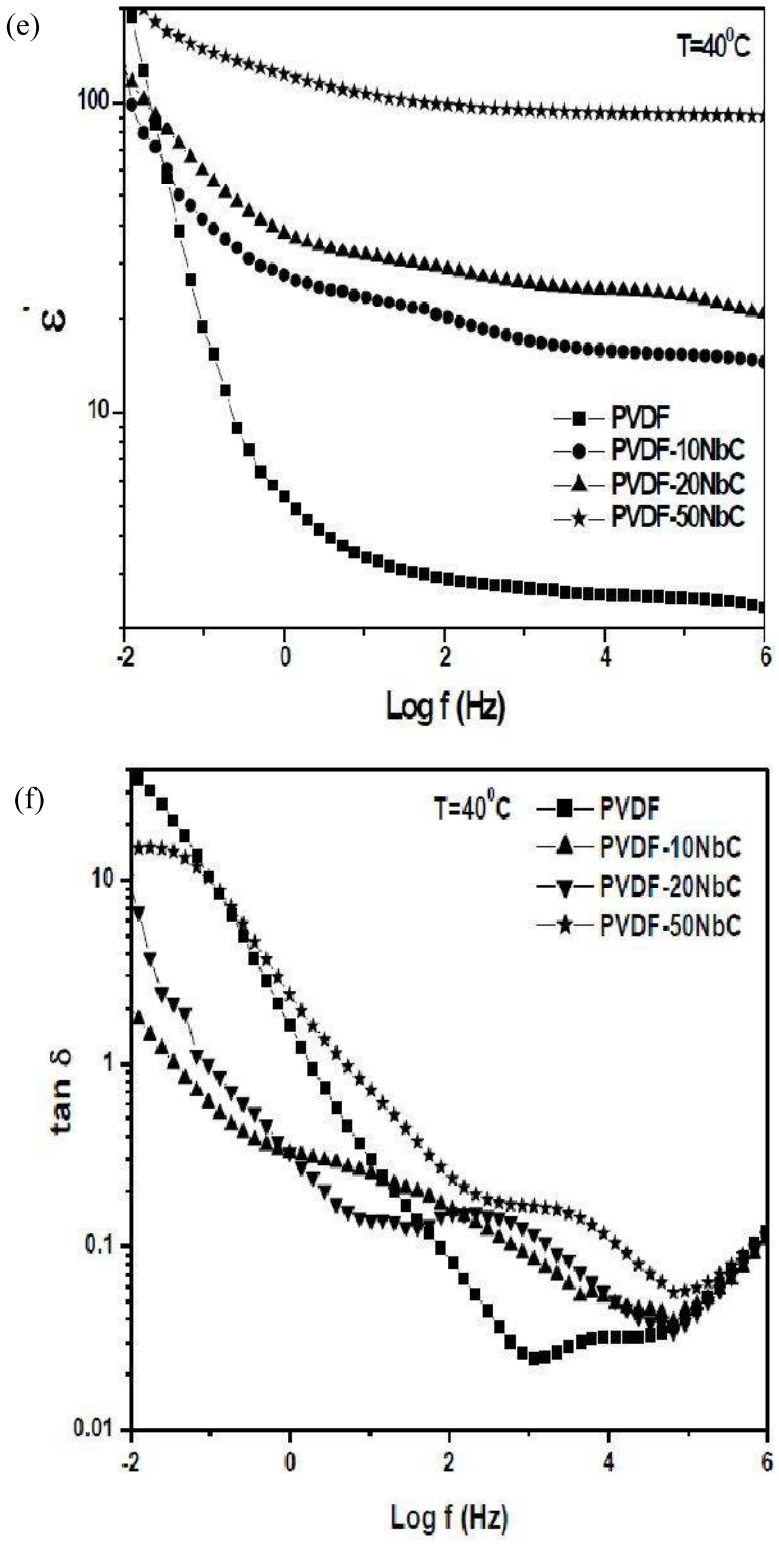

Figure 6.5 Frequency dependence of dielectric permittivity and tan δ (e and f) of PVDF and all the composites at 40^0 C.

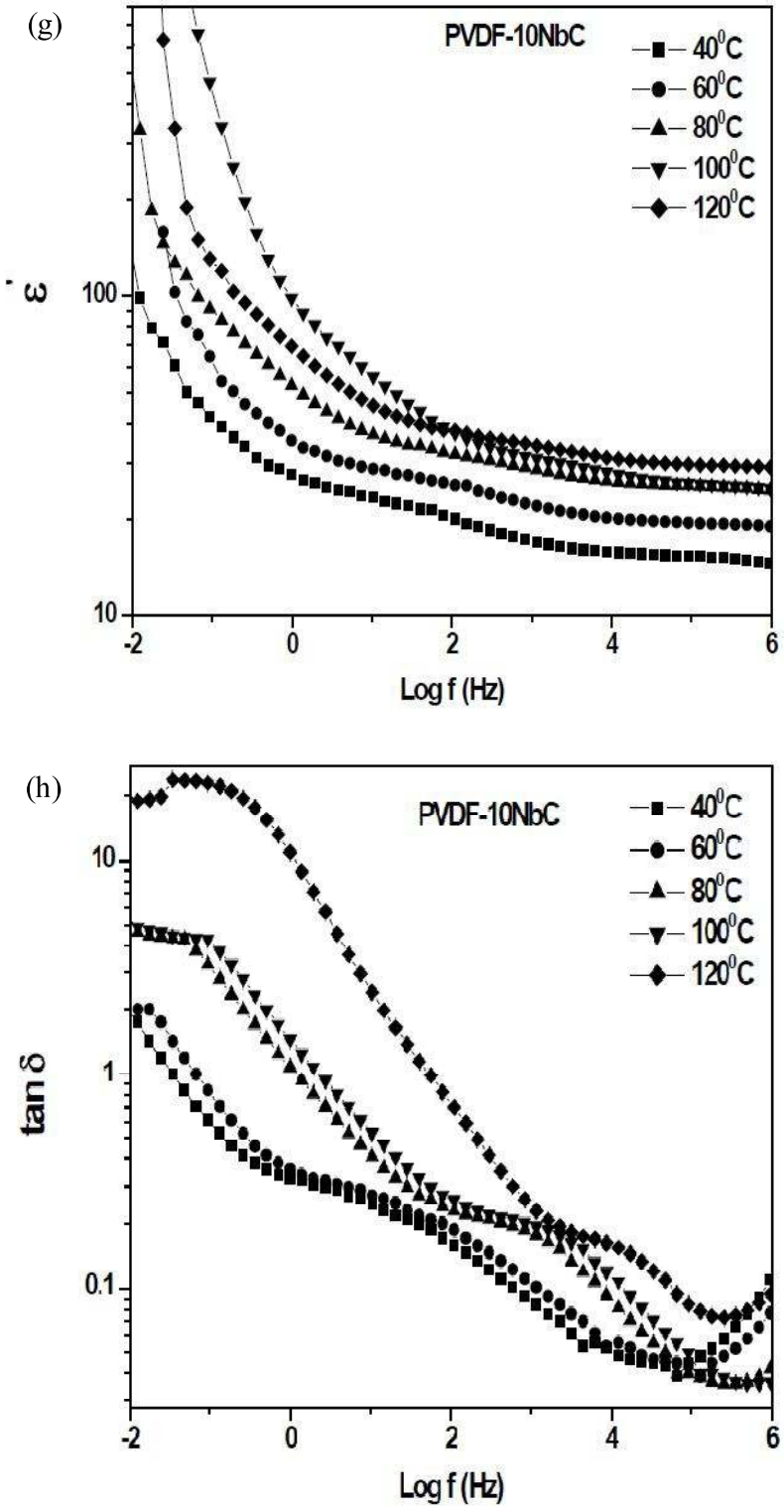

Figure 6.5 Frequency dependence of dielectric permittivity and tan δ (g and h) of PVDF-10NbC at different temperatures.

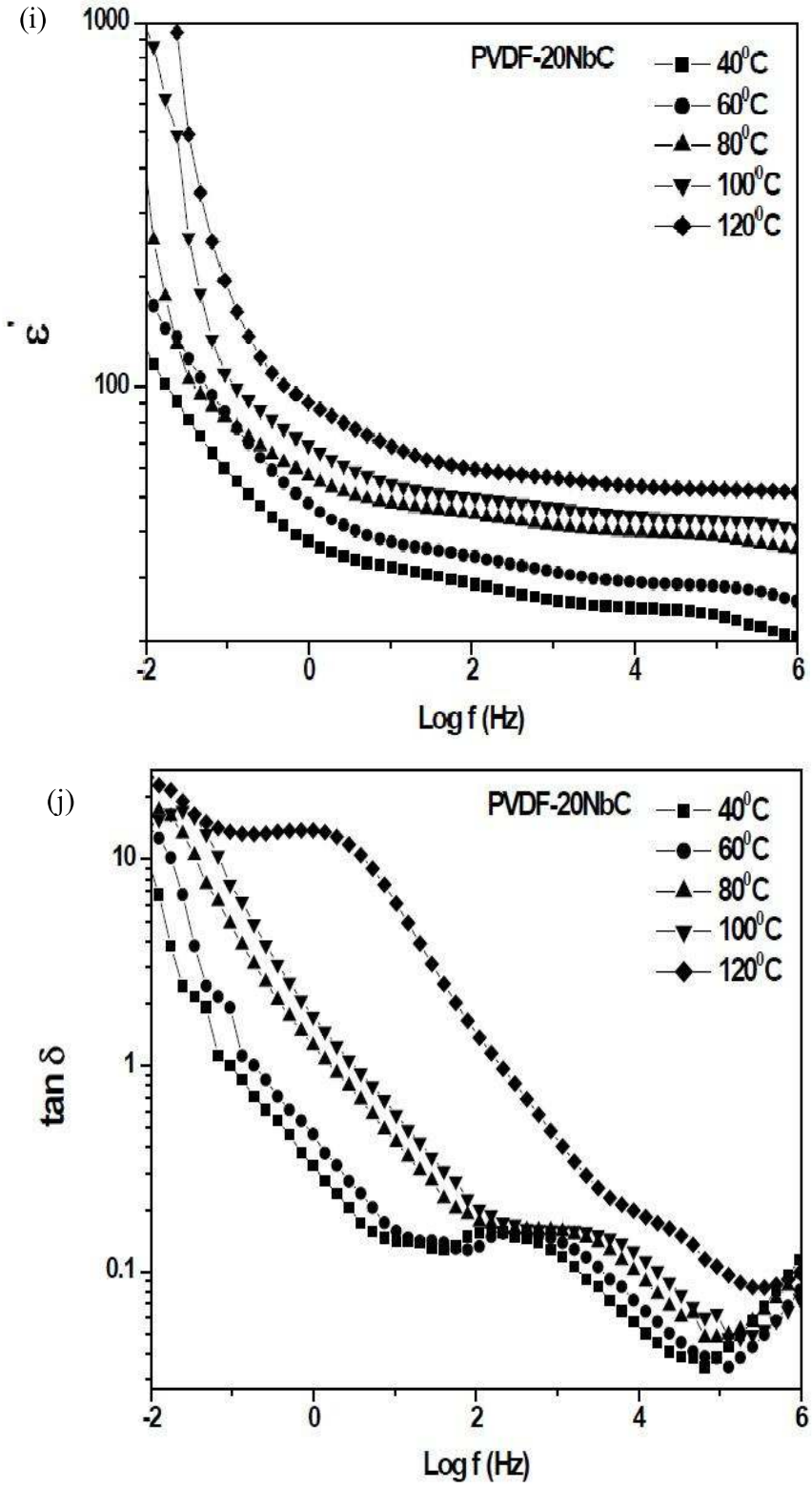

Figure 6.5 Frequency dependence of dielectric permittivity and tan δ (i and j) of PVDF-20NbC at different temperatures.

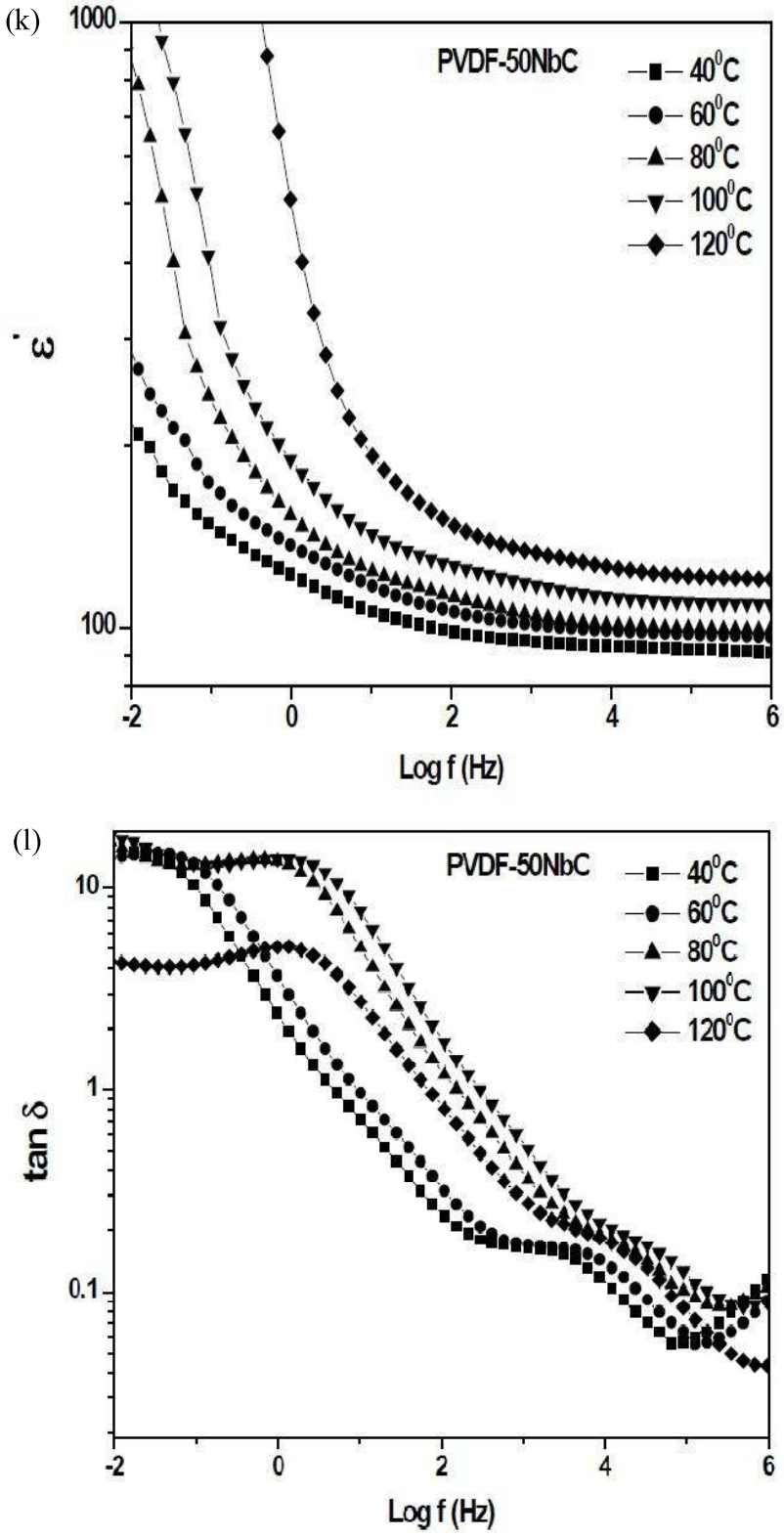

Figure 6.5 Frequency dependence of dielectric permittivity and tan δ (k and l) of PVDF-50NbC at different temperatures.

Frequency dependence of tan δ of CCTO, NbCCTO, PVDF and PVDF-NbC composites is shown in fig 6.5. Tan δ slightly increases from 0.86 in CCTO to 1.68 in NbCCTO at 100 Hz (Fig. 6.5 b). CCTO shows two peaks corresponding to two dielectric relaxation processes. In CCTO one relaxation is present at 0.1 Hz and other at 1 KHz. On Nb doping both the relaxations present in CCTO shift to higher frequency in NbCCTO. Relaxations present at 0.1 Hz and 1 KHz in CCTO shift to 100 Hz and 100 KHz in NbCCTO. The relaxation frequencies for both these dielectric relaxation are higher in NbCCTO than CCTO.

The value of loss tangent for PVDF, PVDF-10NbC, PVDF-20NbC and PVDF-50NbC are 0.09, 0.15, 0.15 and 0.24 at 100 Hz and 40^0C respectively (Fig 6.5 e). In the case of PVDF-NbC composites, one relaxation appears around 10^2 -10^4 Hz while other at a low frequency. At 40^0C and 60^0C it is not visible as it is present at a very low frequency. Above 60^0C, it starts appearing. Low frequency relaxation is due to Maxwell Wagner polarization, while high frequency relaxation is due to α_c relaxation associated with molecular motion of the polymer chains in the crystalline regions of PVDF. The glass transition relaxation α_a of PVDF occurs beyond 1 MHz (Fig 6.5 d) [Gregoria and Cestari (1994); Gregoria and Ueno (1999); Channel and Jog (2008)]. These relaxation peaks shift to higher frequency with increase in temperature (Figs 6.5 h, j and l), indicating lower relaxation time (τ). This seems to be due to the ease of relaxation because of decrease in the viscosity of the polymer with temperature.

To understand the nature of dielectric relaxation modulus spectroscopy has also been used. Electrical modulus is defined as the inverse of complex permittivity.

$$M^* = \frac{1}{\varepsilon^*} = \frac{1}{(\varepsilon' - J\varepsilon'')} = \frac{\varepsilon'}{(\varepsilon'^2 + \varepsilon''^2)} + \frac{J\varepsilon''}{(\varepsilon'^2 + \varepsilon''^2)} = M' + J.M'' \qquad (6.1)$$

where M', ε' and M", ε" are real and imaginary parts of the modulus and permittivity respectively. The real M' and imaginary M" parts of electrical modulus were obtained as a function of frequency [Ramajo et al (2008)]. With dispersion of NbCCTO in PVDF

matrix (Fig 6.6 a), M' decreases. This decrease in M' shows that dielectric permittivity increases with the ceramic reinforcement. This corresponds to the dielectric relaxation process observed in M" vs log f plots (Fig 6.6 c). This relaxation is also observed in PVDF (Fig 6.6 b). Height of the peak decreases with increasing concentration of NbCCTO. With the increase in NbCCTO content this relaxation peak shifts to lower frequency in composites. This is due to restricted mobility of polymeric chains because of their interaction with the filler particles. This shows that the dielectric permittivity as well as the dielectric loss increases with increasing concentration of NbCCTO. The relaxation frequency shifts to higher side with increasing temperature (Figs 6.6 d-f). This relaxation is due to α_c relaxation associated with molecular motion of the polymer chains in the crystalline regions of PVDF.

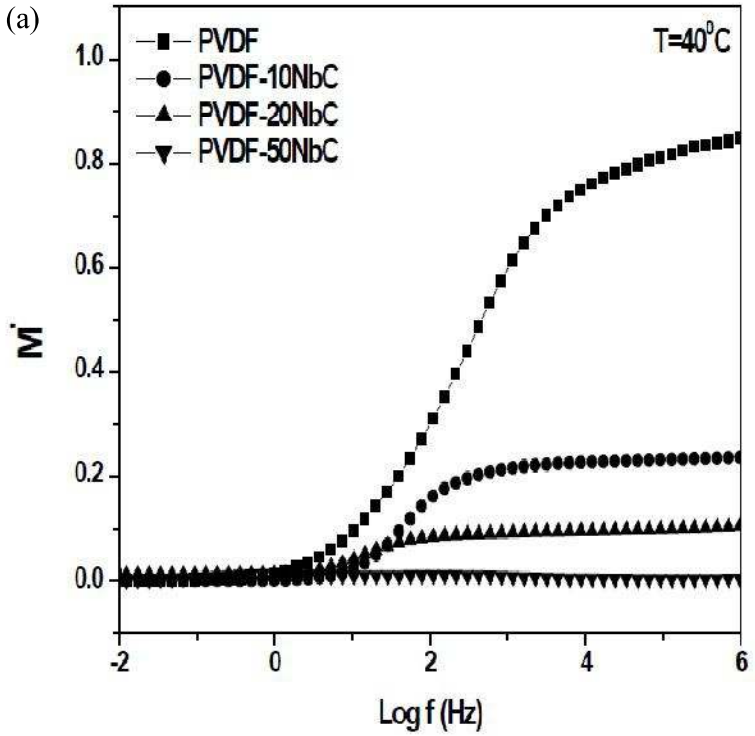

Figure 6.6 (a) M' vs log f plots of PVDF and composites at 40^0 C.

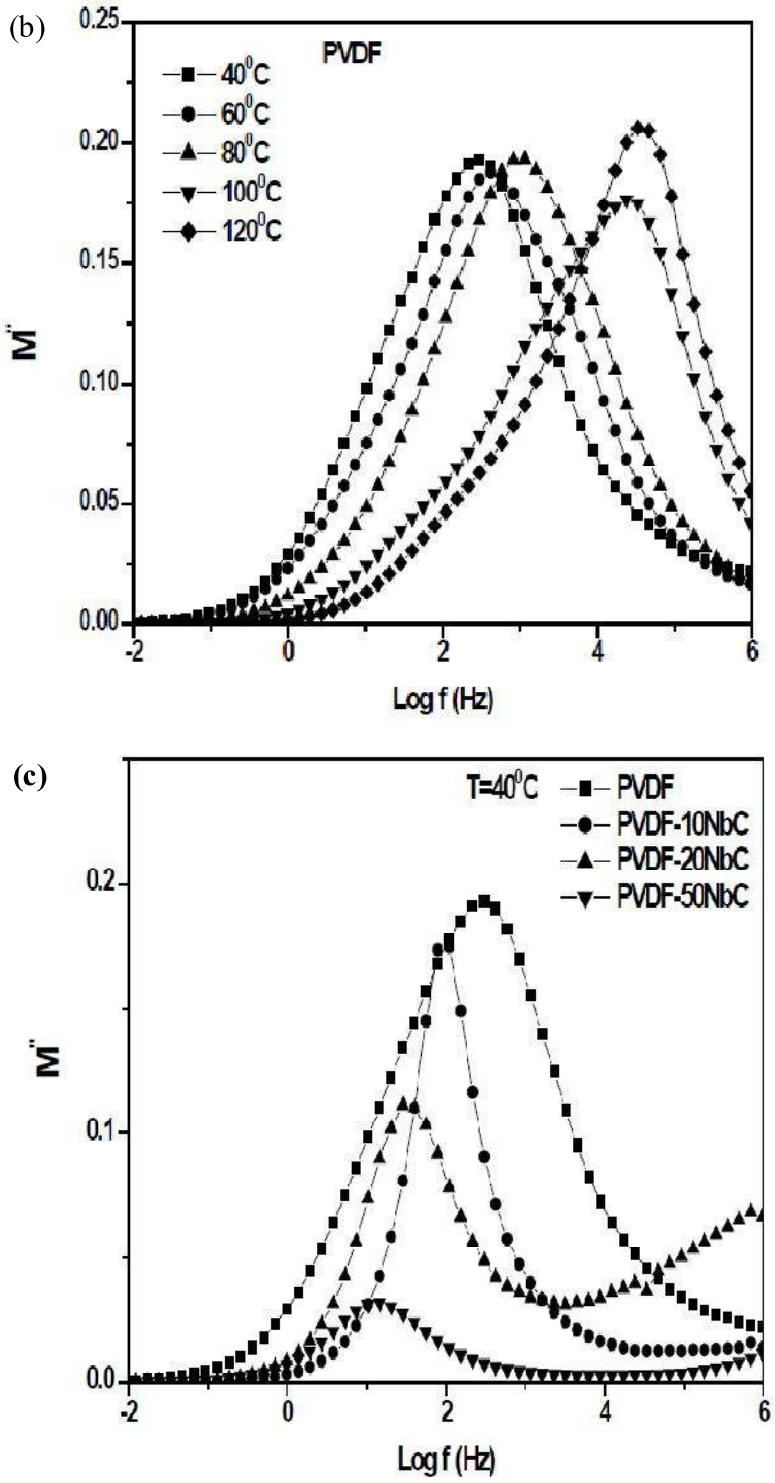

Figure 6.6 M" vs log f plots of (b) PVDF at different temperatures, (c) PVDF and PVDF-NbC composites at 40^0C.

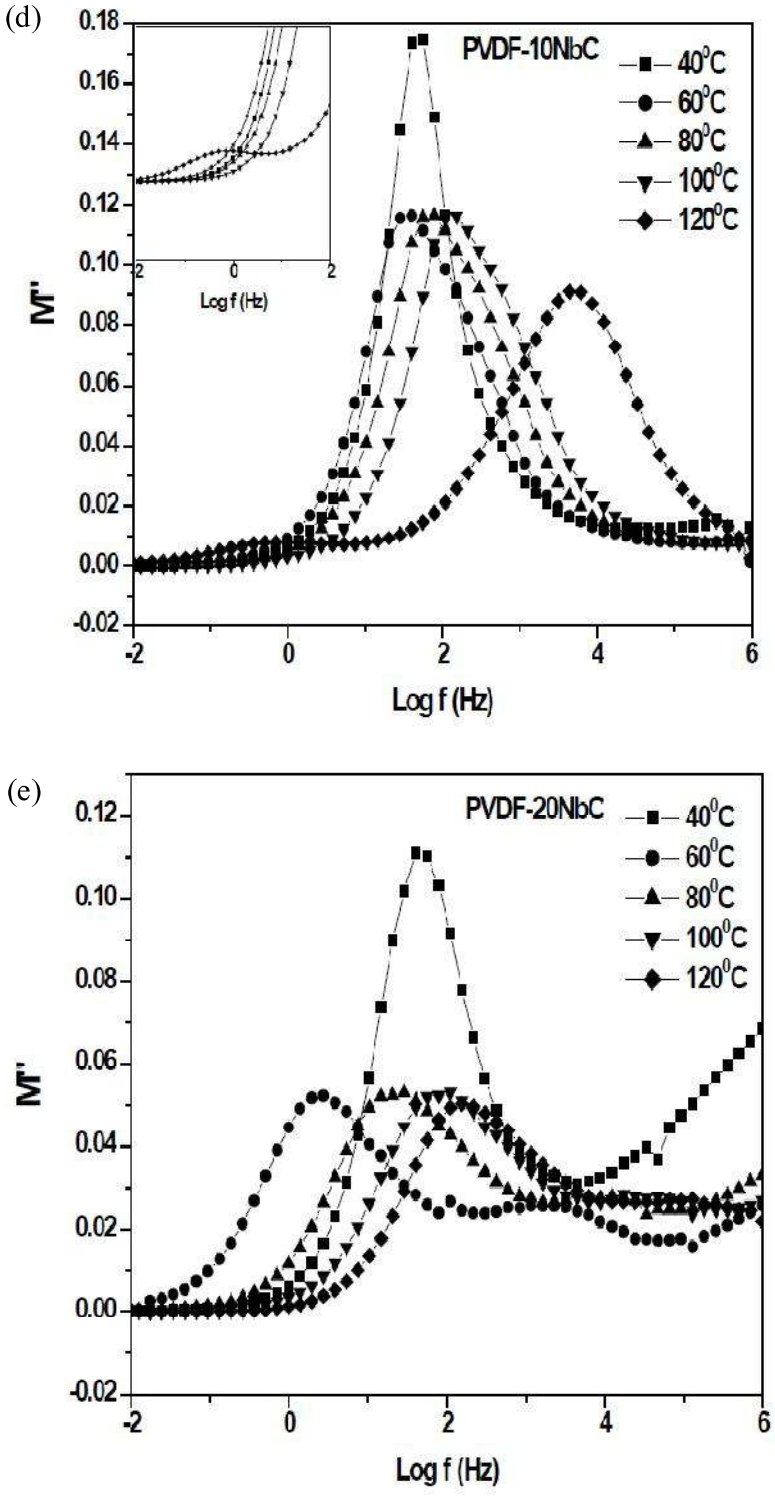

Figure 6.6 M" vs log f plots of (d) PVDF-10NbC at different temperatures, (e) PVDF-20NbC at different temperatures.

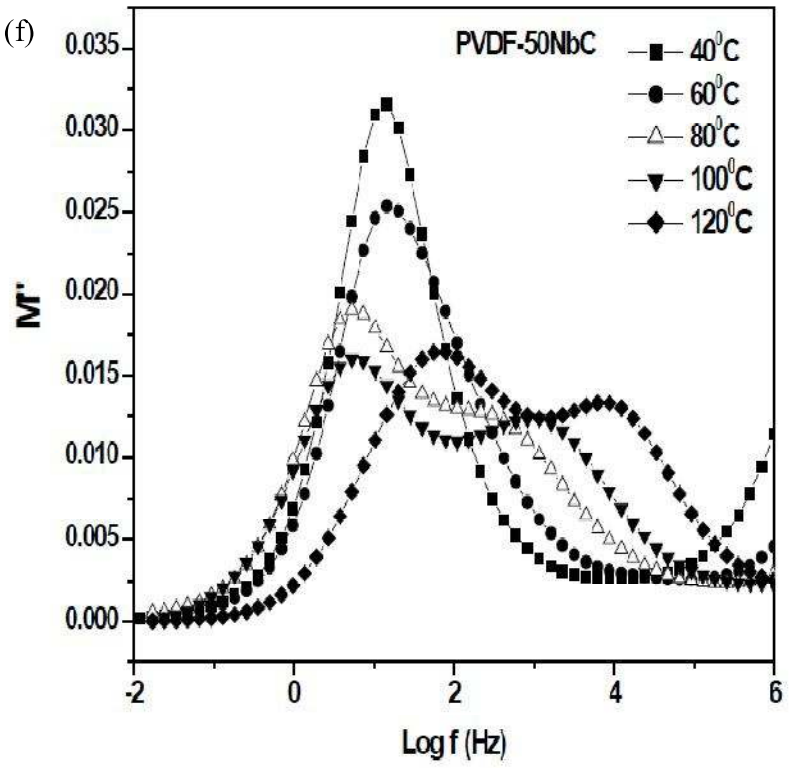

Figure 6.6 M" vs log f plots of (f) PVDF-50NbC at different temperatures.

Figures 6.6 (d-f) show variation of M" vs log f for PVDF-NbC composites at different temperatures. It is observed that another peak appears at low frequency at high temperature. It is not observed in PVDF. This relaxation is of Maxwell-Wagner-Sillar (MWS) type [Ramajo et al (2008); Hedvig (1977)]. Maxwell Wagner Sillar polarization is always present in multiphase systems having phases with different conductivities i.e. electrical heterogeneities. In such materials charge accumulates at the ceramic particles - polymer interface. This gives rise to space charge polarization, which gives high value of dielectric permittivity as well as the dielectric loss. As the dielectric permittivity of NbCCTO is much higher than that of PVDF matrix, unbounded charges form the large dipoles at the polymer matrix – ceramic interface. The induced dipoles find it difficult to follow the alternation of the electric field and thus the resulting relaxation process occurs in the low frequency region or at high temperatures. In PVDF-10NbC α_c relaxation associated with molecular motion of the polymer chains in the crystalline regions of PVDF is present, but Maxwell Wagner polarization is present at a very low frequency,

which is evident only at 120^0C due to the shift at high frequency with increase in temperature. In case of PVDF-20NbC and PVDF-50NbC, relaxation due to Maxwell Wagner polarization and α_c relaxation associated with molecular motion of the polymer chains in the crystalline regions of PVDF are visible above 40^0C. With the increase in temperature both the relaxations shift toward high frequency which indicates decrease in the relaxation time with increasing temperature.

Relaxation times, τ was determined using the relation $\tau = \frac{1}{2\pi f}$ where f is the frequency in cycles per second at the peak position in M" vs log f plots. Plots of log τ vs 1000/T for NbCCTO, PVDF, PVDF-10NbC, PVDF-20NbC and PVDF-50NbC is shown in fig 6.7. These plots are linear in accordance with Arrhenius relationship given below:

$$\tau_{max} = \tau_o \exp(\frac{E_R}{kT}) \qquad (6.2)$$

where E_R is the activation energy associated with the relaxation process, τ_o the pre-exponential factor, k is the Boltzmann constant and T is the absolute temperature. Values of activation energy obtained from the slopes of these linear plots are given in Table 6.1. It is observed that the activation energy for α_c relaxation increases with increasing content of NbCCTO. This may be due to increase in the stiffness with increasing content of NbCCTO.

M" vs log f plots of PVDF and composites (Fig 6.6 c) show that with ceramic dispersion M" peaks shift to low frequency, this indicates the restriction in movement of polymer chains with NbCCTO dispersion. It is also confirmed by tensile test that with the increasing content of NbCCTO, composites become stiffer.

Table 6.1 Activation energy of dielectric relaxation, α_c, relaxation associated with molecular motion of the polymer chains in the crystalline regions of PVDF from M'' vs log f plots.

Sample	Activation Energy
NbCCTO	**0.71 eV**
PVDF	**0.70 eV**
PVDF-10NbC	**0.70 eV**
PVDF-20NbC	**0.81 eV**
PVDF-50NbC	**0.97 eV**

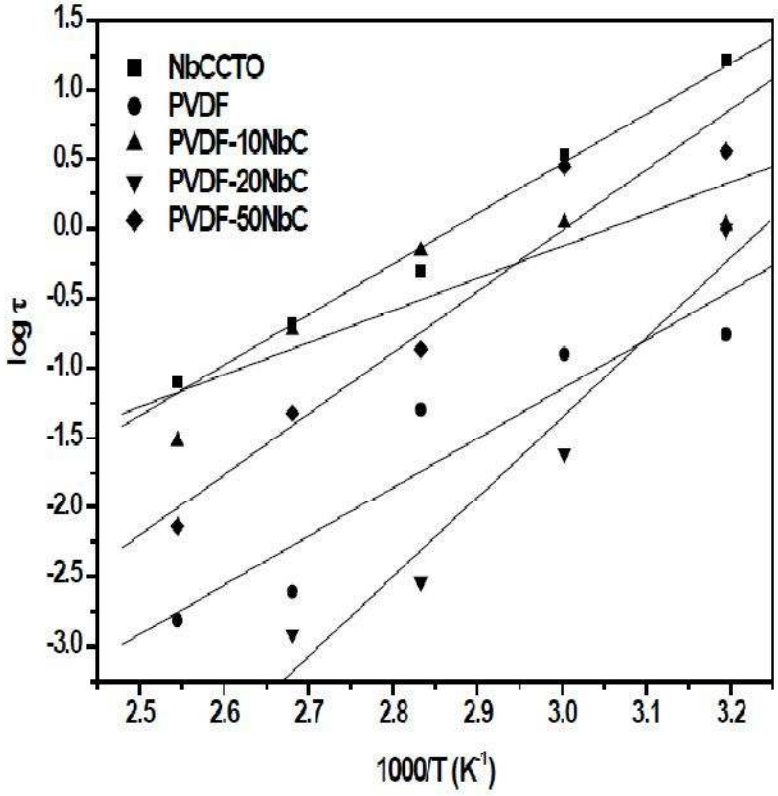

Figure 6.7 Log τ vs 1000/T plots for NbCCTO, PVDF, PVDF-10NbC, PVDF-20NbC and PVDF-50NbC.

To predict the effective dielectric permittivity (ε' or ε_{eff} are the same) of the composites various models are used. The dielectric property of a biphasic dielectric

mixture comprising of spherical crystallites with high dielectric permittivity and a matrix of low dielectric permittivity can be described by Maxwell's model [Maxwell 1954]. According to this model, the effective dielectric permittivity of the composite is given by.

$$\varepsilon_{eff} = \frac{\delta_p \, \varepsilon_p \left(2/3 + \varepsilon_c/3\varepsilon_p\right) + \delta_c \, \varepsilon_c}{\delta_p \left(2/3 + \varepsilon_c/3\varepsilon_p\right) + \delta_c} \qquad (6.3)$$

where, ε_c, ε_p, δ_c and δ_p are the dielectric permittivity of NbCCTO, PVDF, the volume fraction of the ceramic and the polymer respectively. After substituting the values of ε_c, ε_p, δ_c and δ_p, the values of ε_{eff} obtained deviate much from the experimental values for all the volume fractions of NbCCTO under study (Fig 6.8).

In the case of Clausius-Mossotti model [Frolich 1949], it is assumed that the mixture of dielectric is composed of spherical crystallites dispersed in a continuous medium. The effective dielectric permittivity (ε_{eff}) of the composite is given by the following equation.

$$\varepsilon_{eff} = \varepsilon_p \left[1 + 3\delta \left(\frac{(\varepsilon_c - \varepsilon_p)}{\varepsilon_c + 2\varepsilon_p}\right)\right] \qquad (6.4)$$

The predicted value of ε_{eff} using this model also deviates a lot from the experimental values (Fig 6.8).

Lichtenecker's or logarithmic mixture rule is also used to predict the effective value of dielectric permittivity [Nalwa 1995]. According to this model ε_{eff} is given by:

$$\text{Log } \varepsilon_{eff} = \delta_1 log\varepsilon_1 + \delta_2 log\varepsilon_2 \qquad (6.5)$$

Experimental results are significantly different from the predicted results using this model also (Fig 6.8). This is because Logarithmic law is applicable only when there is not much difference in the value of ε' of the dispersion medium and the dispersed phase. This is not true in the case of PVDF-NbC composites.

The effective medium theory (EMT) model [Rao et al (2000] has been developed taking into account the morphology of the particles. According to this model, the ε_{eff} is given by

$$\varepsilon_{eff} = \varepsilon_p[1 + \frac{f_c(\varepsilon_c - \varepsilon_p)}{\varepsilon_p + n(1-f_c)(\varepsilon_c - \varepsilon_p)}] \quad (6.6)$$

where f_c is the volume fraction of the ceramic dispersed, ε_c, ε_p and *n* are the dielectric permittivity of the ceramic, polymer and the ceramic morphology fitting factor respectively. The experimental values obtained are closest to the predicted values in this case of all the models employed to predict the ε_{eff} values. The shape parameter n has been found to be 0.056.

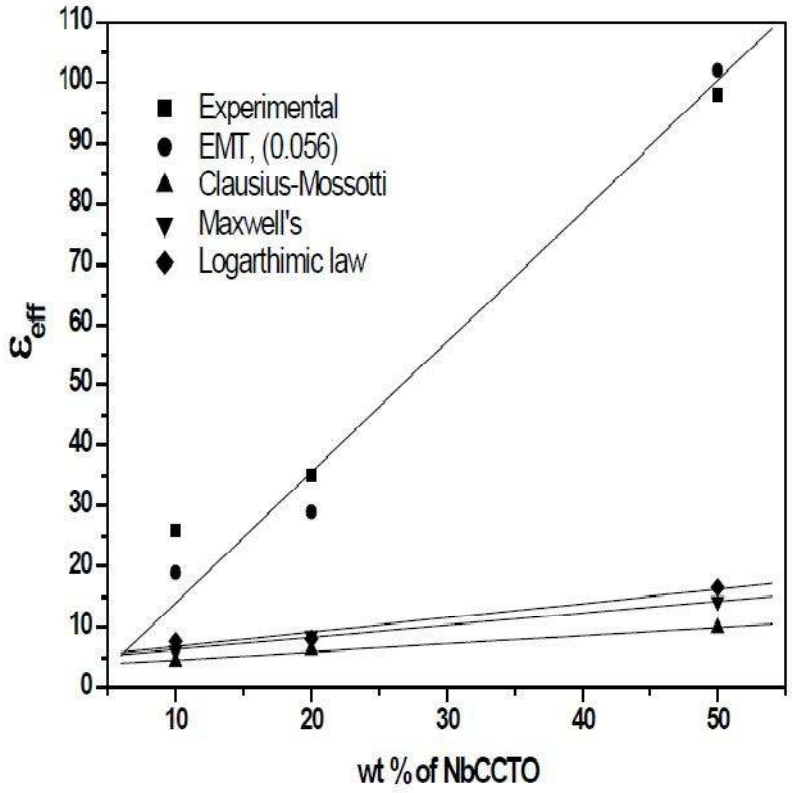

Figure 6.8 Variation of effective dielectric permittivity (ε_{eff}) measured at 100 Hz and 40^{o}C for PVDF-NbC composites based on various models.

All these models have the limitations that the chemistry of interfacial structure has not been taken into account and particles are assumed to be of spherical shape. Microstructure and microchemistry of the interfaces are also very important to determine the physical, mechanical and electrical properties of the composites. Therefore the experimental results do not match exactly with values predicted by these models.

The temperature-dependent dielectric relaxation is explained by Havriliak-Negami (H-N) function [Windlass et al (2001); Mijovic et al (2006)]:

$$\varepsilon^* = -i\frac{\sigma_{dc}}{\varepsilon_0 \omega^s} + \varepsilon_\infty + \sum_j \frac{(\Delta\varepsilon)_j}{[1+(iw\tau_j)^\alpha]^\beta} \qquad (6.7)$$

where, σ_{dc} is dc conductivity, ω is the angular frequency, s is an exponent ($0<s\leq 1$), τ_j is the relaxation time of the j^{th} process, ε_0 is the vacuum permittivity, $\Delta\varepsilon$ is the dielectric strength of the j^{th} process and α and β are the shape parameters of the H-N function which define the symmetric and asymmetric broadening of the α_c relaxation peak in ε'' curve. Analysis of H-N function using WinFit software program of PVDF and PVDF-50NbC composite have been given in Table 6.2 using deconvoluted H-N fits presented in (Fig.6.9). The exponent parameter, α represents the slope of the lower frequency side of the relaxation peak in ε'' curve. β is the asymmetry parameter which is calculated from the slope of higher frequency side of the same curve as α. The higher value of α for composites as compared to pure PVDF indicates a stretched relaxation over a wider range of frequencies whereas $0<\beta\leq 1$ leads to asymmetrical broadening for the relaxation function. For $\beta=1$, the Debye-function is obtained. Asymmetry parameter β has a value of 1 for PVDF showing the symmetry of the spectrum. For the composites, β parameter has different values due to the dispersion of ceramics particles which creates heterogeneity in the system. For composites, the relaxation time (s) calculated from H-N fit decreases with increase in temperature. The composites exhibit lower relaxation time as compared to PVDF. Exact reason for this is not clear at present. With increase in the temperature, the relaxation time decreases in the composites. Lower value of relaxation time at higher temperature is because of the ease of relaxation at higher temperature due to increased mobility of the chains both for pure PVDF as well as composites.

Table 6.2 Fitting parameters for α_c relaxation as a function of temperature obtained from H-N fits.

Temp	PVDF, α	PVDF-50NbC, α	PVDF, β	PVDF-50NbC, β	PVDF, τ	PVDF-50NbC, τ
40^0C	0.49	0.62	1	0.59	2.33E-2	4.32E-2
80^0C	0.53	0.65	1	0.61	1.45E-3	6.26E-3
120^0C	0.57	0.76	1	0.71	7.44E-4	2.18E-5

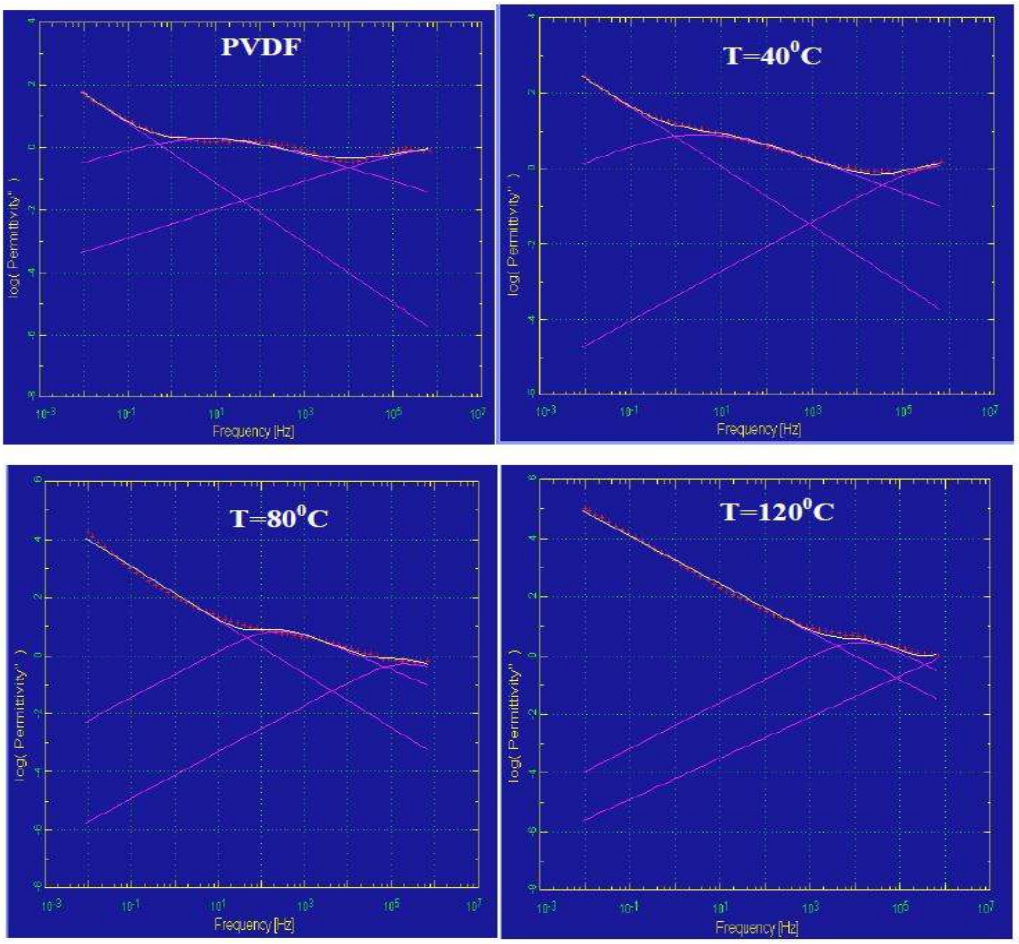

Figure 6.9 Dielectric loss in the frequency domain and spectrum was deconvoluted from H-N fits for PVDF-50NbC.

6.6 Conclusion

- $CaCu_3Ti_4O_{12}$ and Nb doped $CaCu_3Ti_4O_{12}$ (NbCCTO) have been synthesised by solid state conventional technique.

- Composites of PVDF and NbCCTO (PVDF-NbC) have been prepared by melt extrusion process.

- XRD studies indicate no structural change in either polymer or ceramic in the composite but the change in d-spacing indicates better interaction between PVDF and NbCCTO.

- It is found that Young's modulus increases in the composites.

- There is a substantial increase in the dielectric permittivity of CCTO with Nb doping accompanied by a slight increase in dielectric loss.

- Addition of NbCCTO in PVDF increases the dielectric permittivity significantly. In the composites, dielectric loss is slightly more than that in pure PVDF. The relaxation peaks shift towards higher frequencies in the composites suggesting lowering of relaxation time.

- As the filler content increases in the PVDF matrix, M' decreases. In the modulus spectroscopy two dielectric relaxations have been observed in the composites. One relaxation occurring at low frequency is of Maxwell-Wagner-Sillar (MWS) type, while the other relaxation occurring in the high frequency range is due to α_c relaxation associated with molecular motion of the polymer chains in the crystalline regions of PVDF.

- Temperature dependence of dielectric relaxation has been worked out in details through H-N function. Debye type relaxation is observed in pure PVDF with $\beta=1$. Stretched relaxation has been observed over a wider range of frequency in the composite suggesting asymmetric nature of relaxation.